JACS
JOURNAL OF THE AMERICAN CHEMICAL SOCIETY
pubs.acs.org/JACS
Article

Symmetry-Breaking Charge Transfer in Metal−Organic Frameworks

Sreehari Surendran Rajasree, H. Christopher Fry, David J. Gosztola, Bapan Saha, Riya Krishnan, and Pravas Deria*

Cite This: J. Am. Chem. Soc. 2024, 146, 5543−5549
Read Online
ACCESS | Metrics & More | Article Recommendations | Supporting Information

ABSTRACT: High quantum-yield charge carrier generation from the initially prepared excitons defines a key step in the light-harvesting and conversion scheme. Photoinduced charge transfer in molecular electron donor−acceptor assemblies is driven by a sizable ΔG_0, which compromises the potential of the generated carriers. Reminiscent of the special pair at the reaction center of the natural light-harvesting complex, symmetry-breaking charge transfer (SBCT) within a pair of identical struts of metal−organic framework (MOF) will facilitate the efficient generation of long-lived charge carriers with maximized potentials without incorporating any foreign redox species. We report SBCT in pyrene-based zirconium metal−organic framework (MOF) NU-1000 that leads to efficient generation of radical ions in a polar solvent and bound CT states in a low-polar solvent. The probe unveils the role of the low-lying non-Franck−Condon excitonic states as intermediates in the formation of the SBCT state from the initially prepared Franck−Condon S_1 states. Ultrafast and transient spectroscopy—probed over 200 fs-30 μs time scale—evinces a $k_{SBCT} = (110\ ps)^{-1}$ in polar media ($\varepsilon_s = 37.5$) forming solvated radical ions with recombination rate $k_{CR} = (\sim 45\ ns)^{-1}$. A slower rate with $k_{SBCT} = (203\ ps)^{-1}$ was recorded in low-polar ($\varepsilon_s = 7.0$) solvent manifesting a bound [$TBAPy^{\bullet+}$ $TBAPy^{\bullet-}$] state with $k_{CR} \approx (17\ \mu s)^{-1}$. This discovery, along with other unique photophysical features relevant to light harvesting, should define a MOF-based platform for developing heterogeneous artificial photon energy conversion systems.

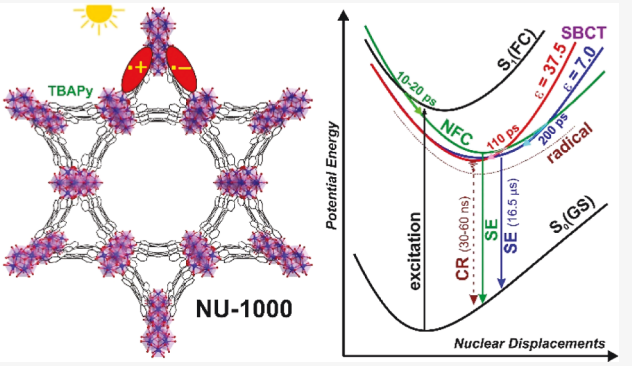

INTRODUCTION

Natural photosynthetic apparatus has provided us with an elegant blueprint of organized pigments for efficient solar energy conversion.[1−3] Within the biological light-harvesting complex (LHC), the excited energy is anisotropically transported from the antennae to the special pair reaction center (RC) to generate charge carriers.[2,4] Maximizing the potential of these carriers, the RC splits the excitons through a unique strategy known as symmetry-breaking charger transfer (SBCT) within a pair of the identical but specifically oriented pair of chlorophylls ($Ch\cdots Ch + h\nu \rightarrow Ch^+ + Ch^-$).[5] This is in stark contrast to the common strategy of exploiting electronically asymmetric (donor−acceptor) pairs with a sizable driving force (ΔG_0), which compromises the potential of the photogenerated charge carriers.[6] While SBCT has been documented with a few molecular pigments in the homogeneous systems,[7−14] they commonly lack various key features of LHC including panchromatic sensitization through a large portion of the visible spectrum[15] and efficient and anisotropic delivery of the excitonic energy (to the RC) producing long-lived redox equivalents.[3,16] Attempts to develop solid molecular compositions featuring most of these functionalities have commonly seen parasitic exciton recombination pathways.[17−21]

Crystalline metal−organic frameworks (MOFs), built out of a wide range of photo- and redox-active pigment-based struts, offer a scalable solid-state foundation for developing an artificial photosynthetic apparatus.[22−26] Such foundations enable precise and periodic arrangement of the active/desired struts around geometrically well-defined pores, which not only suppress aggregation-mediated recombination [of excited state (ES)] but also provide means to modulate the excitonic properties and dynamics relevant to their efficient delivery to "RC" for photoinduced charge-transfer (PCT) processes and catalytic utilities.[27−29] Such developments have further been expanded by various post-synthesis approaches to install a wide range of complementary redox-active entities.[30−39]

Our works have established that MOF singlet ESs can be delocalized with molecular excitons spanning over multiple struts (that are built from aromatic cores like pyrene, porphyrin, phenyl-ethyne-phenyl, etc.).[40] Time-dependent density functional theory (TDDFT)-based computations on

Received: December 6, 2023
Revised: January 27, 2024
Accepted: January 29, 2024
Published: February 14, 2024

https://doi.org/10.1021/jacs.3c13764
J. Am. Chem. Soc. 2024, 146, 5543−5549

small strut assemblies have enabled mapping of the transition density matrix (TDM) which evinced that various excitonic states within the S_1 manifold including the initially prepared Franck−Condon (FC) excitonic state, denoted hereon as S_1(FC), are dispersed over multiple struts (evinced by the diagonal distribution of the excitonic mass). However, such interactions also manifest, within the S_1 manifold, low-energy non-Franck−Condon (NFC) excitonic states and they can be populated from the initial S_1(FC) due to a small energy gap and similar wave functions.[29,40,41] While supramolecular assembly of electron donor−acceptor (D−A) motifs has been extensively exploited for PCT and their subsequent unitilities[6,42−45] in the artificial light-harvesting and conversion schemes,[32,40,46] a systematic and transformative development underpinning the working principle to delineate the unique SBCT strategies in solid-state system like MOF remained unaccomplished. While it is well perceived that the environment plays a critical role in modulating the energy of the SBCT state, spatial overlap of the Frontier orbitals was established as a requirement for dimeric molecular systems.[12,47] Therefore, the dynamics of the SBCT state are tied with the molecular spacing and orientation-a feature that can be precisely defined and controlled by the pore geometry of MOFs which can also instigate a dielectric tuning. Given the spatially dispersed MOF excitonic states, within the S_1 manifold, understanding the role of various NFC states during the S_1(FC) → SBCT process will provide unique insight and direction for further improving and developing MOF-based energy conversion strategies.[8,48]

RESULTS AND DISCUSSION

PCT within an electronically asymmetric chromophore pair has been well established in pyrene [TBAPy: tetrabenzene-carboxypyrene]-based MOF NU-1000 with $k_{PCT} \sim (10-80\ ps)^{-1}$. Owing to the large electronic driving force, these systems compromise the potential energy of the charge carriers (leading to low redox strength or smaller V_{OC} in a photoelectrochemical setup) that recombine with $k_{CR} \sim (300\ ps)^{-1}$.[46,49] However, pigment pairs with comparable electronic potentials have been shown to undergo efficient PCT and slower recombination through exciplex-like intermediate.[50] Such systems are commonly achieved by postsynthetic installation of foreign redox components. Charge carrier generation through SBCT in MOFs featuring spatially dispersed singlet excitons with high and anisotropic mobility will define a significant step forward in artificial photosynthetic systems.

To achieve SBCT within the MOF assemblies of electronically isotropic struts (e.g., all pyrene-based MOFs), the pigment core must possess certain electronic features predicted from the Weller equation[51,52]

$$\Delta G = e(E_{ox} - E_{red}) - E_{00} - C - S \quad (1)$$

$$\left[C \propto {}^{1}/_{\varepsilon_s r_{LL}} \text{ and } S \propto \left({}^{1}/_{r_+} - {}^{1}/_{r_-}\right)\right]$$

where E_{ox} and E_{red} are the electrochemically determined oxidation and reduction potentials; $E_{0,0}$ is the first excitation energy;[53] and C and S are the Coulombic interactions between the two ions and their solvation correction terms, respectively. Coulombic interaction is inversely dependent on the solvent dielectrics. From these, it is expected that a small driving force can arise from the Coulombic term if the anionic radius (r_-) is larger than that of the cation (r_+).

In brief, an increase in solvent polarity will make the latter term more negative to facilitate the CT process. From the Weller equation, a sizable driving force can be obtained for struts whose optical band gap is slightly larger than their electrochemical band gap. By screening various aromatic pigment-based MOFs, TBAPy assembly of NU-1000 (Figure 1a) was picked for which the experimentally measured $E_{0,0}$ = 2.83 eV; $E_{ox} - E_{red}$ = 2.09 V; and $r_{LL} \sim 10.9$ Å. From these metrics, ΔG of −0.88 and −0.9 eV as well as solvent reorganization energy, λ_s[54] of 1.10 and 0.75 eV can be estimated in ε = 7.0 (e.g., MeTHF) and ε = 37.5 (e.g., MeCN and dimethylformamide) solvents.[55] Considering solvent-independent internal reorganization energy (λ_i = 0.39 eV), a relative contribution of the exponential term in the Marcus rate equation[56,57] can be obtained using equation 2.

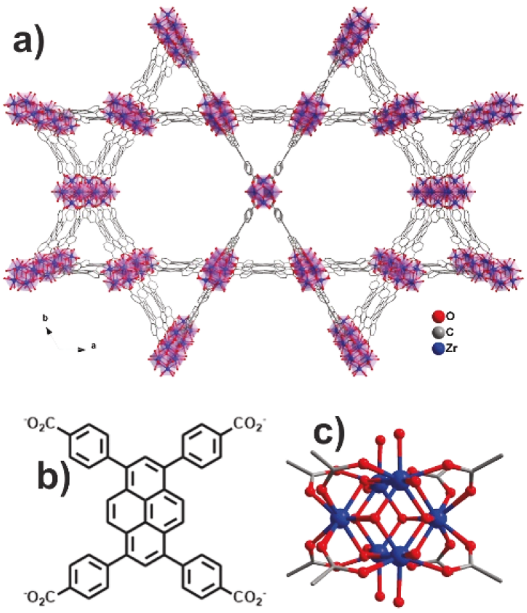

Figure 1. a) Chemical structure of NU-1000 and its constituent linker, (b) TBAPy, and (c) 8-connected Zr-oxo node. The structure highlights the hierarchical 1D pore system that anisotropically aligns the linkers along a triangular pore (d = 10 Å) defining excitonic sites.[41]

$$k_e \propto H_{CT}{}^2 \exp\left[-\frac{(\lambda_t + \Delta G^0)^2}{4\pi\lambda_t k_b T}\right] \quad (2)$$

This indicated that the k_e in ε = 7.0 solvent can be ca. 1.25× larger than that in ε = 37.5 media assuming a constant H_{CT} ($=\langle\psi_{SBCT}|\hat{H}_{CT}|\psi_{S_1(FC)}\rangle$), which is the electronic coupling matrix element for precursor and product states). Here, λ_t is the total reorganization energy ($=\lambda_i + \lambda_s$).

To probe SBCT in NU-1000, solvent-dielectric-dependent ($\varepsilon_s \sim 7-38$) transient spectroscopic experiments were carried out. Figure 2 displays the respective data. The femtosecond transient absorption (fs-TA) data collected for the unassembled TBAPy (ester form) strut in solution (ε = 7.0; MeTHF) display an intense excited-state absorption (ESA) at 710 nm and a broad near-infrared ESA in the 900−1200 nm region with a monotonous single species-based dynamics (τ = 2 ns; Figure 2a). In contrast, the spectral signature of NU-1000 in ε = 7.0 medium revealed that the initially prepared S_1(FC) population (characterized by the red-shifted $S_1 \rightarrow S_n$

https://doi.org/10.1021/jacs.3c13764
J. Am. Chem. Soc. 2024, 146, 5543−5549

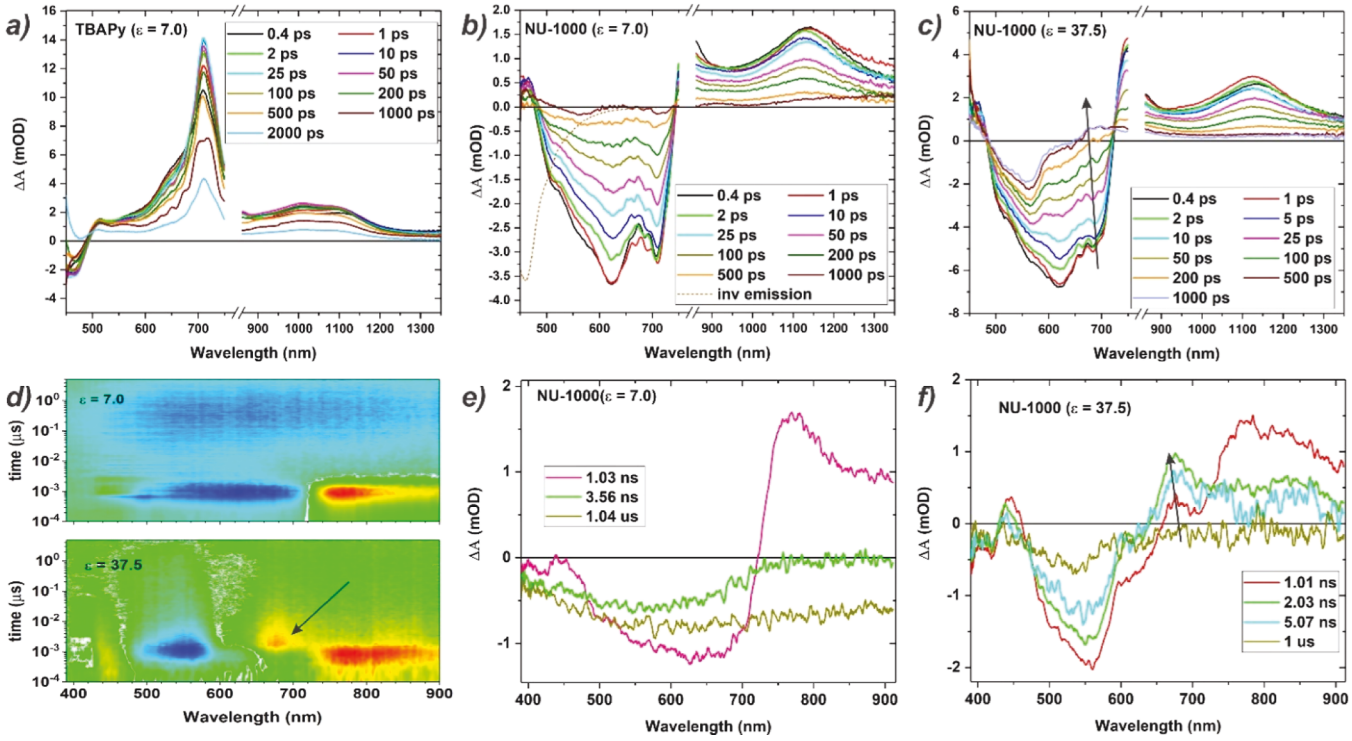

Figure 2. Dielectric-dependent transient absorption spectra: (a) fs-TA spectra of Et_4TBAPy in MeTHF solvent showing the $S_1 \rightarrow S_n$ transitions at 710 and broad 1000−1100 nm region, (b) NU-1000 in a low-polar solvent (dotted line is inverted emission) showing 500−725 nm SE from NFC states, (c) NU-1000 in polar solvent showing a quicker decay of the SE at ∼650−700 nm region (arrow) due to the appearance of positive TA signal for $TBAPy^{\bullet+}$ and $TBAPy^{\bullet-}$ radical ions, and (d) color map for ns-TA of NU-1000 showing the evolution of SE from SBCT state in low polar and TA signal (arrow) of radical ions formed in polar solvent. (e,f) Corresponding ns-TA spectra at various delay times showing the narrow SE band caused by the rise of radical-ion signals (arrow) in polar solvent.

transitions appearing at ∼750−850 and 1150 nm) quickly (<0.4 ps) populates an ensemble of low-energy NFC states characterized by the broad (500−750 nm) SE bands appearing significantly read to the spontaneous emission band (at 470 nm, with shoulders at 500 and 550 nm; Figure 2b). The entire spectral envelope of SE from the NFC states recovers—followed further through the nanosecond transient absorption spectroscopy (ns-TA)—eventually to a species with a featureless broad spectral envelope of the SE signal that spans beyond 920 nm. This long-lived state is insensitive to oxygen quenching (Figures S5 and S6) and recombines over 15 μs. Based on these, the long-lived featureless band is assigned to an SBCT state that can be envisioned as a bound [$TBAPy^{\bullet+}$ $TBAPy^{\bullet-}$] pair. Global fitting of the transient spectroscopic data (both fs-TA and ns-TA; see Supporting Information, Section F) provides τ = 14 ps, 203 ps, 1 ns, and 17 μs time constants in MeTHF solvent. Based on the emissive lifetime (∼1 ns) and quantum yield [∼45%; a sizable S_1(FC) population will continue displaying the $S_1 \rightarrow S_n$ signal causing a mixed-state spectral signature in the EAS/SAS plots], these lifetimes can be attributed to τ[S_1(FC) → NFC] = 14 ps; τ[NFC → SBCT] = 203 ps, emissive decay τ [$S_1 \rightarrow$ GS] = 1 ns; and τ[SBCT → GS] = 17 μs. The SBCT state did not manifest any spectral signature for the radical-ion species.

In contrast, the spectral evolution of TBAPy assemblies within NU-1000 in polar solvent (ε = 37.5) was significantly different: the ensemble of NFC state efficiently populated to the SBCT state which partly manifests solvated radical ions, at an early stage, as evinced by an unsymmetrical recovery of the broad SE band due to a quicker disappearance of low-energy side with the emergence of an ESA signal at ∼680 nm (Figure 2c).[46,58] The radical-ion signature can be seen in the ns-TA mapping data (Figure 2d), with a narrow SE emission band (Figure 2f). Similar global fitting of the transient spectroscopic data collected in MeCN solvent provides (see Supporting Information, Section F) time constants attributed to τ[S_1(FC) → NFC] = 11 ps; τ[NFC → SBCT] = 110 ps, emissive decay τ[$S_1 \rightarrow$ GS] ≃ 2 ns (see Figure S4 for fluorescence lifetimes and Figures S7 and S8 for the fit); and two time constants for the recovery of the SBCT states: one from the radical ion pair τ[SBCT(radical) → GS] ≃ 45 ns and from the bound pair with broad featureless SE, τ[SBCT → GS] ≃ 6.5 μs (Figure S10). Within the Marcus framework (eq 2), reorganization energy plays a dominant role for space-separated donor−acceptor pairs (from a neutral D*−A/D−A* pair in the S_1(FC) state to a charge pair D^+−A^- in the SBCT state), predicting an efficient process in low dielectric media. However, transient spectroscopic data indicates that the polar solvent not only facilitates the SBCT formation but can also stabilize the radical-ion state. Since the S_1(FC) state in NU-1000 is delocalized over many TBAPy struts with excitonic sites defined by the three TBAPy struts around each triangular pore, the process can be considered as a radiation-less transition of the initially prepared S_1(FC) population to the SBCT state of a given superchromophore[41] and will scale with $\exp[-(\Delta E_{S_1(FC)-SBCT} - \lambda)^2/\lambda]$. This transition will be further facilitated by the involvement of a low-energy NFC intermediate state with small reorganization and $\Delta E_{NFC-SBCT}$ energy gap [i.e., S_1(FC) → NFC → SBCT]. For that an

https://doi.org/10.1021/jacs.3c13764
J. Am. Chem. Soc. 2024, 146, 5543−5549

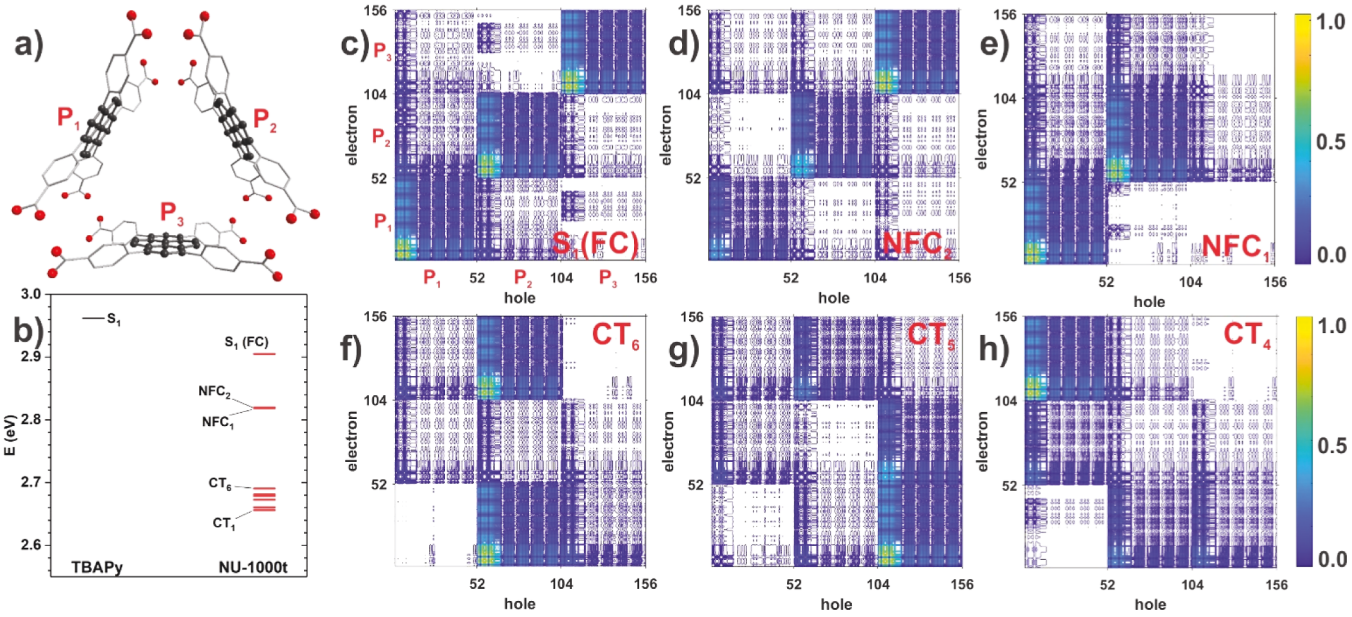

Figure 3. a) Trimeric TBAPy assembly of NU-1000 used for TDDFT computation proving the (b) energy for the S_1(FC), NFC, and CT states at the GS-optimized geometry; the S_1 energy for an unassembled TBAPy strut is given for comparison. Contour plots of TDMs for various ESs: (c) S_1(FC) [marked P_i is the TBAPy strut shown in (a), each with 52 atoms as numbered in the axes], (d,e) NFC states, and (f–h) CT_6, CT_5, and CT_4 states. The colors represent the densities normalized to 1.

efficient S_1(FC) → NFC transition was observed with $\tau \sim 11-15$ ps owing to a small $\Delta E_{S_1(FC)-NFC}$.

To shed some light on the ES species, a small triangular model consisting of three TBAPy struts—defining one excitonic site—was used for TDDFT (see Supporting Information, Section G for details) computation.[41] The TDDFT-computed energies on the ground-state (GS)-optimized structure (i.e., vertical excitation) of these excitonic states are plotted in Figure 3b. Based on the oscillator strengths and the corresponding excitonic mass distribution in the, respective, TDM plots, the ninth state was assigned as the S_1(FC), right below which (eighth and seventh) are the two NFC states named NFC_1 and NFC_2 and followed by six SBCT states, CT_6–CT_1 (Figure 3b).[59] The excitonic mass distribution in the, respective, TDM plots (Figure 3d,e) suggests that the NFC_1 and NFC_2 states can be described as $|^1(P_1{\cdot}P_2{\cdot}P_3)^*\rangle$, $|^1(P_1{\cdot}P_2)^*{\cdot}P_3\rangle$, and so on; where P_1, P_2, and P_3 are the adjacent TBAPy pigments in a triangular model (Figure 3a). Notably, the NFC_2 ($|^1(P_1{\cdot}P_2)^*{\cdot}P_3\rangle$) state[60] describes an excimer-like complex that can be a good precursor for the SBCT state.[61] Among the six lower-energy SBCT states, only CT_4 (Figure 3h) denotes an ionic state described by $|P_1^+{\cdot}P_2{\cdot}P_3^-\rangle$ with asymmetrically distributed (non-diagonal) excitonic mass and the rest of the CT_n states can be described as partial charge-distributed states, like $|P_1^+{\cdot}P_2^{\delta-}{\cdot}P_3^{\delta-}\rangle$, $|P_1^{\delta+}{\cdot}P_2^{\delta+}{\cdot}P_3^-\rangle$, and so on (Figures 3 and S13).

The NFC → SBCT transitions can be understood from the energies of the ES relaxed geometry (i.e., TDDFT/opt),[8] where among the six CT_n states, the highest energy CT_6 can be considered as the initial transition point from the lowest-energy NFC_1 state. For the S_1(FC) → NFC → SBCT transition, the energy variation for the, respective, states was probed: the $\Delta E_{S1(FC)-NFC}$ = 0.058 eV at GS-optimized structure, which increases (0.11 eV) at the ES-optimized geometry at which a nominal $\Delta E_{NFC-CT6} = 6 \times 10^{-3}$ eV was found (Figures S14 and S15).[48] It is therefore clear that despite a sizable energy gap between the initial S_1(FC) and final SBCT states, the NFC state, as an intermediate, can tunnel the population: it has a small energy gap with the initially prepared S_1(FC) state in the GS-optimized geometry (i.e., upon vertical excitation) and a small gap with the SBCT state upon relaxation. TDDFT-based ES optimization implementing a polarizable continuum model for different dielectric media (tetrahydrofuran and MeCN) suggests that the energies of the (see Figure S15) CT_4 state are significantly stable in a polar solvent and destabilized in a nonpolar solvent which also feature a larger $\Delta E_{NFC-CT6} = 11 \times 10^{-3}$ eV (compared to that evinced for ε = 37.5). This explains the observation of a faster SBCT formation rate (100 ps^{-1}) leading to radical-ion signature in polar solvent (ε = 37.5) where low dielectric media can only manifest SE from the bound partially polarized states. Based on these computational and experimental data, the processes are summarized in Figures 4 and S16.

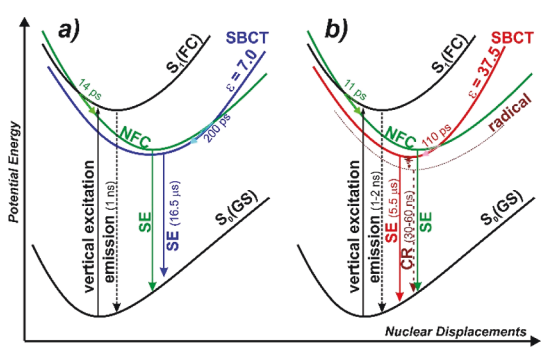

Figure 4. Potential energy surfaces describing the ES processes involved in SBCT within NU-1000 in (a) low (ε = 7)- and (b) high (ε = 37.5)-polar solvents. See Figure S15 for the TDDFT-computed energies of the GS- and ES-optimized structures.

https://doi.org/10.1021/jacs.3c13764
J. Am. Chem. Soc. 2024, 146, 5543–5549

CONCLUSIONS

Interchromophoric interaction within the MOF-assembled organic pigment/struts gives rise to several excitonic states within the S_1 manifold including the initially prepared FC excitonic states, S_1(FC), and lower-energy NFC excitonic states, which can be populated from the initial S_1(FC). The extent of the excitonic mass distribution and, respective, nuclear coordinates varies for these states: for example, while the S_1(FC) states are spatially dispersed, some of the low-energy NFC states can be anisotropic, defining excimer-like and CT states. Pigment-based struts with $E_{0,0} > E_{redox}$ and with anionic radius (r_-) larger than the cation (r_+) could produce SBCT states, whose energy and potential surface can be modulated by the dielectric environment defined by the infiltrated solvent, whereas the interpigment interaction and, therefore, the dynamics of the SBCT states can be dictated by the pore geometry. Within this context, pyrene-assembled NU-1000 showed efficient SBCT formation. While predicted observations from the classic electron-transfer theory suggested that a low dielectric media can be beneficial for SBCT formation, transient spectroscopic results evince that the polar solvent not only facilitates the SBCT formation but also can stabilize the radical-ion state. Given that the initially prepared S_1(FC) state in NU-1000 is delocalized over many TBAPy struts with excitonic sites defined by the three TBAPy struts around each triangular pore, the S_1(FC) → SBCT transition can be described as a radiation-less transition between two states where involvement of NFC state plays a critical role tunneling the population owing to the small energy gap and reorganization energy at the GS structure [for S_1(FC) → NFC] and ES relaxed structure (for NFC → SBCT). Time-dependent DFT computation suggests the formation of various SBCT states defined by the variable extent of asymmetric charge distribution, among which the radical ion pair state is more stable in polar solvent, enabling spectroscopic identification. In polar media, the efficient formation [k_{SBCT} = (110 ps)$^{-1}$] of the persisting radical-ion state [k_{CR} = (45 ns)$^{-1}$] represents a remarkable feature for developing artificial photosynthetic solids within such MOFs forming long-lived usable charge carriers. The discovery, therefore, highlights a rich vein of unique photophysics that has been eluding solid compositions: SBCT in MOF can be modulated by the optoelectronic property of the pigment itself and by the pore geometry of the frameworks that precisely defines and controls the interpigment distance and orientation. Such structural features not only enable exceptionally mobile spatially dispersed singlet excitons but also can dictate how they will be split, i.e., the dynamics of the SBCT and the extent of charge transfer (radical ions vs bound pairs) even within MOFs constructed from a single pigment−corollary that is simply difficult to achieve in solution-dissolved macromolecular systems.

ASSOCIATED CONTENT

Supporting Information

The Supporting Information is available free of charge at https://pubs.acs.org/doi/10.1021/jacs.3c13764.

Experimental details and computational and additional spectroscopic data (PDF)

AUTHOR INFORMATION

Corresponding Author

Pravas Deria − *School of Chemical and Biomolecular Science, Southern Illinois University, Carbondale, Illinois 62901, United States;* orcid.org/0000-0001-7998-4492; Email: pderia@siu.edu

Authors

Sreehari Surendran Rajasree − *School of Chemical and Biomolecular Science, Southern Illinois University, Carbondale, Illinois 62901, United States*

H. Christopher Fry − *Center for Nanoscale Materials, Argonne National Laboratory, Lemont, Illinois 60439, United States;* orcid.org/0000-0001-8343-5189

David J. Gosztola − *Center for Nanoscale Materials, Argonne National Laboratory, Lemont, Illinois 60439, United States;* orcid.org/0000-0003-2674-1379

Bapan Saha − *School of Chemical and Biomolecular Science, Southern Illinois University, Carbondale, Illinois 62901, United States;* orcid.org/0000-0002-8138-3618

Riya Krishnan − *School of Chemical and Biomolecular Science, Southern Illinois University, Carbondale, Illinois 62901, United States*

Complete contact information is available at: https://pubs.acs.org/10.1021/jacs.3c13764

Notes

The authors declare no competing financial interest.

ACKNOWLEDGMENTS

P.D. gratefully acknowledges funding from the National Science Foundation (NSF CAREER CHE-1944903). Use of the Center for Nanoscale Materials, an Office of Science user facility, was supported by the U.S. Department of Energy, Office of Science, Office of Basic Energy Sciences, under Contract no. DE-AC02-06CH11357. Scanning electron microscopy−energy-dispersive spectroscopy data were collected at the SIUC IMAGE center (supported by NSF grant #CHE0959568).

REFERENCES

(1) Scholes, G. D.; Fleming, G. R.; Olaya-Castro, A.; van Grondelle, R. Lessons from Nature about Solar Light Harvesting. *Nat. Chem.* **2011**, *3*, 763−774.

(2) Damjanović, A.; Ritz, T.; Schulten, K. Energy transfer between carotenoids and bacteriochlorophylls in light-harvesting complex II of purple bacteria. *Phys. Rev. E* **1999**, *59*, 3293−3311.

(3) Barber, J.; Andersson, B. Revealing the Blueprint of Photosynthesis. *Nature* **1994**, *370*, 31−34.

(4) Brinkert, K. *Energy Conversion in Natural and Artificial Photosynthesis*; Springer, 2018.

(5) Deisenhofer, J.; Norris, J. R. *The Photosynthetic Reaction Center*; Academic Press, Inc., 1993.

(6) Wasielewski, M. R. Photoinduced Electron Transfer in Supramolecular Systems for Artificial Photosynthesis. *Chem. Rev.* **1992**, *92*, 435−461.

(7) Sebastian, E.; Hariharan, M. Symmetry-Breaking Charge Separation in Molecular Constructs for Efficient Light Energy Conversion. *ACS Energy Lett.* **2022**, *7*, 696−711.

(8) Piet, J. J.; Schuddeboom, W.; Wegewijs, B. R.; Grozema, F. C.; Warman, J. M. Symmetry Breaking in the Relaxed S1 Excited State of Bianthryl Derivatives in Weakly Polar Solvents. *J. Am. Chem. Soc.* **2001**, *123*, 5337−5347.

(9) Fritz, R.; Rettig, W.; Nishiyama, K.; Okada, T.; Müller, U.; Müllen, K. Excitonic and Charge Transfer States in Oligomeric 9,10-Anthrylene Chains. *J. Phys. Chem. A* **1997**, *101*, 2796−2802.
(10) Giaimo, J. M.; Lockard, J. V.; Sinks, L. E.; Scott, A. M.; Wilson, T. M.; Wasielewski, M. R. Excited Singlet States of Covalently Bound, Cofacial Dimers and Trimers of Perylene-3,4:9,10-bis-(dicarboximide)s. *J. Phys. Chem. A* **2008**, *112*, 2322−2330.
(11) Markovic, V.; Villamaina, D.; Barabanov, I.; Lawson Daku, L. M.; Vauthey, E. Photoinduced Symmetry-Breaking Charge Separation: The Direction of the Charge Transfer. *Angew. Chem., Int. Ed.* **2011**, *50*, 7596−7598.
(12) Estergreen, L.; Mencke, A. R.; Cotton, D. E.; Korovina, N. V.; Michl, J.; Roberts, S. T.; Thompson, M. E.; Bradforth, S. E. Controlling Symmetry Breaking Charge Transfer in BODIPY Pairs. *Acc. Chem. Res.* **2022**, *55*, 1561−1572.
(13) Whited, M. T.; Patel, N. M.; Roberts, S. T.; Allen, K.; Djurovich, P. I.; Bradforth, S. E.; Thompson, M. E. Symmetry-Breaking Intramolecular Charge Transfer in the Excited State of Meso-Linked BODIPY Dyads. *Chem. Commun.* **2012**, *48*, 284−286.
(14) Sebastian, E.; Hariharan, M. Null Exciton-Coupled Chromophoric Dimer Exhibits Symmetry-Breaking Charge Separation. *J. Am. Chem. Soc.* **2021**, *143*, 13769−13781.
(15) Trinh, C.; Kirlikovali, K.; Das, S.; Ener, M. E.; Gray, H. B.; Djurovich, P.; Bradforth, S. E.; Thompson, M. E. Symmetry-Breaking Charge Transfer of Visible Light Absorbing Systems: Zinc Dipyrrins. *J. Phys. Chem. C* **2014**, *118*, 21834−21845.
(16) Wasielewski, M. R. Photoinduced electron transfer in supramolecular systems for artificial photosynthesis. *Chem. Rev.* **1992**, *92*, 435−461.
(17) Wasielewski, M. R. Self-Assembly Strategies for Integrating Light Harvesting and Charge Separation in Artificial Photosynthetic Systems. *Acc. Chem. Res.* **2009**, *42*, 1910−1921.
(18) Prathapan, S.; Johnson, T. E.; Lindsey, J. S. Building-block synthesis of porphyrin light-harvesting arrays. *J. Am. Chem. Soc.* **1993**, *115*, 7519−7520.
(19) Hasobe, T.; Kashiwagi, Y.; Absalom, M. A.; Sly, J.; Hosomizu, K.; Crossley, M. J.; Imahori, H.; Kamat, P. V.; Fukuzumi, S. Supramolecular Photovoltaic Cells Using Porphyrin Dendrimers and Fullerene. *Adv. Mater.* **2004**, *16*, 975−979.
(20) Sengupta, S.; Würthner, F. Chlorophyll J-Aggregates: From Bioinspired Dye Stacks to Nanotubes, Liquid Crystals, and Biosupramolecular Electronics. *Acc. Chem. Res.* **2013**, *46*, 2498−2512.
(21) Kim, D.; Osuka, A. Directly Linked Porphyrin Arrays with Tunable Excitonic Interactions. *Acc. Chem. Res.* **2004**, *37*, 735−745.
(22) Feng, D.; Gu, Z.-Y.; Li, J.-R.; Jiang, H.-L.; Wei, Z.; Zhou, H.-C. Zirconium-Metalloporphyrin PCN-222: Mesoporous Metal-Organic Frameworks with Ultrahigh Stability as Biomimetic Catalysts. *Angew. Chem., Int. Ed.* **2012**, *51*, 10307−10310.
(23) Mondloch, J. E.; Bury, W.; Fairen-Jimenez, D.; Kwon, S.; DeMarco, E. J.; Weston, M. H.; Sarjeant, A. A.; Nguyen, S. T.; Stair, P. C.; Snurr, R. Q.; Farha, O. K.; Hupp, J. T. Vapor-Phase Metalation by Atomic Layer Deposition in a Metal-Organic Framework. *J. Am. Chem. Soc.* **2013**, *135*, 10294−10297.
(24) Jiang, H.-L.; Feng, D.; Wang, K.; Gu, Z.-Y.; Wei, Z.; Chen, Y.-P.; Zhou, H.-C. An Exceptionally Stable, Porphyrinic Zr Metal-Organic Framework Exhibiting pH-Dependent Fluorescence. *J. Am. Chem. Soc.* **2013**, *135*, 13934−13938.
(25) Lan, G.; Li, Z.; Veroneau, S. S.; Zhu, Y.-Y.; Xu, Z.; Wang, C.; Lin, W. Photosensitizing Metal-Organic Layers for Efficient Sunlight-Driven Carbon Dioxide Reduction. *J. Am. Chem. Soc.* **2018**, *140*, 12369−12373.
(26) Rajasree, S. S.; Li, X.; Deria, P. Physical properties of porphyrin-based crystalline metal-organic frameworks. *Commun. Chem.* **2021**, *4*, 47.
(27) Li, X.; Surendran Rajasree, S.; Yu, J.; Deria, P. The Role of Photoinduced Charge Transfer for Photocatalysis, Photoelectrocatalysis and Luminescence Sensing in Metal-Organic Frameworks. *Dalton Trans.* **2020**, *49*, 12892−12917.
(28) Deria, P.; Yu, J.; Smith, T.; Balaraman, R. P. Ground-State versus Excited-State Interchromophoric Interaction: Topology Dependent Excimer Contribution in Metal-Organic Framework Photophysics. *J. Am. Chem. Soc.* **2017**, *139*, 5973−5983.
(29) Yu, J.; Anderson, R.; Li, X.; Xu, W.; Goswami, S.; Rajasree, S. S.; Maindan, K.; Gómez-Gualdrón, D. A.; Deria, P. Improving Energy Transfer within Metal−Organic Frameworks by Aligning Linker Transition Dipoles along Framework Axis. *J. Am. Chem. Soc.* **2020**, *142*, 11192−11202.
(30) Karagiaridi, O.; Bury, W.; Mondloch, J. E.; Hupp, J. T.; Farha, O. K. Solvent-Assisted Linker Exchange: An Alternative to the *De Novo* Synthesis of Unattainable Metal-Organic Frameworks. *Angew. Chem., Int. Ed.* **2014**, *53*, 4530−4540.
(31) Takaishi, S.; DeMarco, E. J.; Pellin, M. J.; Farha, O. K.; Hupp, J. T. Solvent-Assisted Linker Exchange (SALE) and Post-Assembly Metallation in Porphyrinic Metal-Organic Framework Materials. *Chem. Sci.* **2013**, *4*, 1509−1513.
(32) Goswami, S.; Yu, J.; Patwardhan, S.; Deria, P.; Hupp, J. T. Light Harvesting "Antenna" Behavior in NU-1000. *ACS Energy Lett.* **2021**, *6*, 848−853.
(33) Van Wyk, A.; Smith, T.; Park, J.; Deria, P. Charge-Transfer within Zr-Based Metal-Organic Framework: The Role of Polar Node. *J. Am. Chem. Soc.* **2018**, *140*, 2756−2760.
(34) Williams, D. E.; Dolgopolova, E. A.; Godfrey, D. C.; Ermolaeva, E. D.; Pellechia, P. J.; Greytak, A. B.; Smith, M. D.; Avdoshenko, S. M.; Popov, A. A.; Shustova, N. B. Fulleretic Well-Defined Scaffolds: Donor-Fullerene Alignment Through Metal Coordination and Its Effect on Photophysics. *Angew. Chem., Int. Ed.* **2016**, *55*, 9070−9074.
(35) Song, Y.; Li, Z.; Zhu, Y.; Feng, X.; Chen, J. S.; Kaufmann, M.; Wang, C.; Lin, W. Titanium Hydroxide Secondary Building Units in Metal-Organic Frameworks Catalyze Hydrogen Evolution under Visible Light. *J. Am. Chem. Soc.* **2019**, *141*, 12219−12223.
(36) Lin, S.; Cairnie, D. R.; Davis, D.; Chakraborty, A.; Cai, M.; Morris, A. J. Photoelectrochemical alcohol oxidation by mixed-linker metal-organic frameworks. *Faraday Discuss.* **2021**, *225*, 371−383.
(37) Liu, X.; Kozlowska, M.; Okkali, T.; Wagner, D.; Higashino, T.; Brenner-Weiß, G.; Marschner, S. M.; Fu, Z.; Zhang, Q.; Imahori, H.; Bräse, S.; Wenzel, W.; Wöll, C.; et al. Photoconductivity in Metal-Organic Framework (MOF) Thin Films. *Angew. Chem., Int. Ed.* **2019**, *58*, 9590−9595.
(38) Dolgopolova, E. A.; Rice, A. M.; Smith, M. D.; Shustova, N. B. Photophysics, Dynamics, and Energy Transfer in Rigid Mimics of GFP-based Systems. *Inorg. Chem.* **2016**, *55*, 7257−7264.
(39) Choi, S.; Jung, W.-J.; Park, K.; Kim, S.-Y.; Baeg, J.-O.; Kim, C. H.; Son, H.-J.; Pac, C.; Kang, S. O. Rapid Exciton Migration and Amplified Funneling Effects of Multi-Porphyrin Arrays in a Re(I)/Porphyrinic MOF Hybrid for Photocatalytic CO2 Reduction. *ACS Appl. Mater. Interfaces* **2021**, *13*, 2710−2722.
(40) Yu, J.; Park, J.; Van Wyk, A.; Rumbles, G.; Deria, P. Excited-State Electronic Properties in Zr-Based Metal−Organic Frameworks as a Function of a Topological Network. *J. Am. Chem. Soc.* **2018**, *140*, 10488−10496.
(41) Rajasree, S. S.; Yu, J.; Pratik, S. M.; Li, X.; Wang, R.; Kumbhar, A. S.; Goswami, S.; Cramer, C. J.; Deria, P. Superradiance and Directional Exciton Migration in Metal-Organic Frameworks. *J. Am. Chem. Soc.* **2022**, *144*, 1396−1406.
(42) Lee, C. Y.; Farha, O. K.; Hong, B. J.; Sarjeant, A. A.; Nguyen, S. T.; Hupp, J. T. Light-Harvesting Metal-Organic Frameworks (MOFs): Efficient Strut-to-Strut Energy Transfer in Bodipy and Porphyrin-Based MOFs. *J. Am. Chem. Soc.* **2011**, *133*, 15858−15861.
(43) Dolgopolova, E. A.; Williams, D. E.; Greytak, A. B.; Rice, A. M.; Smith, M. D.; Krause, J. A.; Shustova, N. B. A Bio-inspired Approach for Chromophore Communication: Ligand-to-Ligand and Host-to-Guest Energy Transfer in Hybrid Crystalline Scaffolds. *Angew. Chem., Int. Ed.* **2015**, *54*, 13639−13643.
(44) Fang, Z.-B.; Liu, T.-T.; Liu, J.; Jin, S.; Wu, X.-P.; Gong, X.-Q.; Wang, K.; Yin, Q.; Liu, T.-F.; Cao, R.; Zhou, H.-C. Boosting Interfacial Charge-Transfer Kinetics for Efficient Overall CO2 Photoreduction via Rational Design of Coordination Spheres on

https://doi.org/10.1021/jacs.3c13764
J. Am. Chem. Soc. 2024, 146, 5543−5549

Metal-Organic Frameworks. *J. Am. Chem. Soc.* **2020**, *142*, 12515−12523.
(45) Xia, Z.; He, C.; Wang, X.; Duan, C. Modifying electron transfer between photoredox and organocatalytic units via framework interpenetration for β-carbonyl functionalization. *Nat. Commun.* **2017**, *8*, 361.
(46) Van Wyk, A.; Smith, T.; Park, J.; Deria, P. Charge-Transfer within Zr-Based Metal−Organic Framework: The Role of Polar Node. *J. Am. Chem. Soc.* **2018**, *140*, 2756−2760.
(47) Lee, C.; Choi, C. H.; Joo, T. A Solvent-Solute Cooperative Mechanism for Symmetry-Breaking Charge Transfer. *Phys. Chem. Chem. Phys.* **2020**, *22*, 1115−1121.
(48) Roy, P.; Bressan, G.; Gretton, J.; Cammidge, A. N.; Meech, S. R. Ultrafast Excimer Formation and Solvent Controlled Symmetry Breaking Charge Separation in the Excitonically Coupled Subphthalocyanine Dimer. *Angew. Chem., Int. Ed.* **2021**, *60*, 10568−10572.
(49) Li, X.; Yu, J.; Gosztola, D. J.; Fry, H. C.; Deria, P. Wavelength-Dependent Energy and Charge Transfer in MOF: A Step toward Artificial Porous Light-Harvesting System. *J. Am. Chem. Soc.* **2019**, *141*, 16849−16857.
(50) Li, X.; Yu, J.; Lu, Z.; Duan, J.; Fry, H. C.; Gosztola, D. J.; Maindan, K.; Rajasree, S. S.; Deria, P. Photoinduced Charge Transfer with a Small Driving Force Facilitated by Exciplex-like Complex Formation in Metal-Organic Frameworks. *J. Am. Chem. Soc.* **2021**, *143*, 15286−15297.
(51) Rehm, D.; Weller, A. Kinetics of Fluorescence Quenching by Electron and H-Atom Transfer. *Isr. J. Chem.* **1970**, *8*, 259−271.
(52) Weller, A. Photoinduced Electron Transfer in Solution: Exciplex and Radical Ion PairFormation Free Enthalpies and their Solvent Dependence. *Z. Phys. Chem.* **1982**, *133*, 93−98.
(53) $E_{0,0}$ values determined from the crossing point of their normalized lowest energy absorption and fluorescence spectra.
(54) The solvent reorganization energy (λ_s) for the bulk solvent was calculated by the Marcus relation:[55] $\lambda_s = \frac{e^2}{4\pi\epsilon_0}\left(\frac{1}{2r_D} + \frac{1}{2r_A} - \frac{1}{r_{DA}}\right)\left(\frac{1}{n^2} - \frac{1}{\varepsilon_s}\right)$ where, is the permittivity of free space, the static dielectric constant of the solvent, n is the refractive index, and e is the magnitude of the charge of an electron; and are the effective radius of the cation (3.02 Å) and the anion (7.1 Å), respectively.
(55) Marcus, R. A. On the Theory of Electron-Transfer Reactions. VI. Unified Treatment for Homogeneous and Electrode Reactions. *J. Chem. Phys.* **1965**, *43*, 679−701.
(56) Coropceanu, V.; Cornil, J.; da Silva Filho, D. A.; Olivier, Y.; Silbey, R.; Brédas, J. L. Charge Transport in Organic Semiconductors. *Chem. Rev.* **2007**, *107*, 926−952.
(57) Marcus, R. A. On The Theory of Electrochemical and Chemical Electron Transfer Processes. *Can. J. Chem.* **1959**, *37*, 155−163.
(58) Kung, C.-W.; Wang, T. C.; Mondloch, J. E.; Fairen-Jimenez, D.; Gardner, D. M.; Bury, W.; Klingsporn, J. M.; Barnes, J. C.; Van Duyne, R.; Stoddart, J. F.; Wasielewski, M. R.; Farha, O. K.; Hupp, J. T. Metal-Organic Framework Thin Films Composed of Free-Standing Acicular Nanorods Exhibiting Reversible Electrochromism. *Chem. Mater.* **2013**, *25*, 5012−5017.
(59) A larger model, two triangular unit with six struts can be used with the expense of computation time resulting proportionally 36th state as the S_1(FC) which delocalized over all six TBAPy units forming two excitonic sites.
(60) And other possible ones like $|^1(P_1{}^*{\cdot}P2{\cdot}P_3)\rangle$ in larger model.
(61) Miller, C. E.; Wasielewski, M. R.; Schatz, G. C. Modeling Singlet Fission in Rylene and Diketopyrrolopyrrole Derivatives: The Role of the Charge Transfer State in Superexchange and Excimer Formation. *J. Phys. Chem. C* **2017**, *121*, 10345−10350.

https://doi.org/10.1021/jacs.3c13764
J. Am. Chem. Soc. 2024, 146, 5543−5549